Date: 8/19/2022
Submission to: *Journal of Membrane Science*

Facile synthesis of nanofiltration membrane with asymmetric selectivity towards enhanced water recovery for groundwater remediation

Wulin Yang,[1,2#] Li Long,[2#] Hao Guo,[2] Chenyue Wu,[2] Shenghua Zhou,[2] Ying Mei,[2] Lu Elfa Peng,[2] Wenyu, Liu,[2] Zhe Yang,*[2] Wanbin Li,[2,3] Chuyang Y. Tang*[2]

[1]College of Environmental Sciences and Engineering, Peking University, Beijing 100871, China.

[2]Department of Civil Engineering, The University of Hong Kong, Pokfulam, Hong Kong SAR, China.

[3]Guangdong Key Laboratory of Environmental Pollution and Health, School of Environment, Jinan University, Guangzhou 511443, China.

[#]Wulin Yang and Li Long contributed equally

*Corresponding author: Zhe Yang, zheyang@connect.hku.hk, +852 2857 8470

Chuyang Y. Tang, tangc@hku.hk, +852 28591976

ABSTRACT

Groundwater remediation by nanofiltration (NF) membrane is still hindered by low water recovery due to membrane scaling. In this study, a simple NaOH-promoted interfacial polymerization strategy was proposed to tailor the membrane asymmetric selectivity of calcium over sulfate ions to reduce scaling potential towards high water recovery. A 0.5 wt% NaOH was introduced during the interfacial polymerization of piperazine (PIP) and trimesoyl chloride on a polysulfone support. The promoted interfacial polymerization reduced polyamide defects for better rejection and enabled use of lower PIP concentrations. Enhanced hydrolysis of polyamide layer created a more negatively charged surface with larger pore sizes to achieve asymmetrical selectivity together with enhanced permeance. The water permeance of fabricated TFC-0.1 membrane with the aid of NaOH was 2.1 times of that for commercial NF270 membrane, while exhibiting comparable perfluorooctanesulfonic acid rejections (>95%). This membrane also achieved ~50% more water recovery than that for NF270 membrane under simulated gypsum scaling condition, owing to the selective passage of calcium (low rejection of 11.4 ± 0.6%). The exemplified strategy of NaOH-promoted interfacial polymerization is facile and readily scalable, which demonstrated strong potential towards high water recovery in groundwater remediation contaminated by emerging pollutants.

KEYWORDS: polyamide membranes, nanofiltration, promoted interfacial polymerization, asymmetrical selectivity, scaling resistance

INTRODUCTION

Groundwater contamination by emerging pollutants has drawn great concerns in recent years [1-5]. Emerging contaminants such as perfluoroalkyl substances (PFASs) were found widespread and persistent in groundwater systems due to their high chemical resistance to environmental degradation processes [5-8]. Perfluorooctanesulfonate (PFOS), an important type of PFASs, has been found at varying concentrations up to 70.1 ng L^{-1} in water environment worldwide [9]. PFOS is bioaccumulative and toxic at trace concentrations, posing potential adverse effects on human health [10, 11]. Therefore, the removal of PFOS from groundwater is critical for environmental remediation.

Nanofiltration (NF) has been applied as an effective separation technology to remove PFOS from groundwater [12-16]. Compared to other membrane processes such as reverse osmosis, NF can be operated at relatively low pressure (<10 bar) with less energy consumption while still maintaining a relatively high rejection of PFOS (>95%) [15, 17-19]. Despite the high removal efficiency of PFOS, scaling of NF membranes limits the water recovery during remediation [20, 21]. Groundwater usually contains high levels of divalent ions such as calcium, magnesium and sulfate that are often well rejected by conventional NF membranes (e.g., > 95% for sulfate and 50~95% for calcium, see Figure 1A) [22-24]. At high water recovery, the accumulation and supersaturation of these ions in the brine can lead to severe membrane scaling (e.g., by calcium sulfate dihydrate, gypsum), which greatly reduces water flux [25-28]. In addition, excessive rejection of calcium may deplete the mineral content of the treated water, causing it more corrosive and less suitable for drinking purpose [29].

To overcome the selectivity limitation of conventional NF membranes, we envision a novel NF membrane with asymmetrical selectivity, such that calcium can freely pass through the

asymmetrically selective membrane while sulfate and PFOS are adequately removed (Figure 1B). This strategy would effectively divert Ca^{2+} and SO_4^{2-} into the permeate and the brine, respectively, thereby mitigating the risk of scaling and addressing the drinking water quality at the same time. The selectivity of an NF membrane is mainly regulated by size exclusion and charge interaction [30-32]. However, size exclusion is not an effective way to achieve asymmetrical selectivity due to its non-discriminative nature (e.g., reducing the pore size of the membrane would enhance the rejection of all species). In contrast, designing a negatively charged membrane surface is critical to ensure discriminatively high rejection of PFOS and sulfate anions. A recent study reported a negatively charged NF membrane with alleviated gypsum fouling by grafting sulfonate groups on membrane surface, obtaining low Ca^{2+} rejection of ~6% but decreased $SO4^{2-}$ rejections to 57.5% [33]. Another study fabricated a negatively charged NF membrane solely using 2,2′-benzidinedisulfonic acid as the aqueous reactant and achieved ~ 5.7% rejection of Ca^{2+} with inhibited gypsum scaling, but also decreased $SO4^{2-}$ rejections to ~45% [34]. A simultaneous increase in membrane pore size can be adopted to further reduce the rejection of calcium and to enhance the membrane permeance, thereby overcoming the longstanding permeance-selectivity tradeoff [35].

This study reports a simple NaOH-promoted interfacial polymerization to fabricate asymmetrically selective NF membranes. We take advantage of the catalytic effect of sodium hydroxide during interfacial reaction (Figure S3), to effectively reduce the formation of nanosized defects in the polyamide layer – an intrinsic problem of interfacial polymerization [36]. At the same time, NaOH can partially hydrolyze the polyamide layer to create a more negatively charged rejection layer with larger effective pore size, thereby achieving asymmetrical selectivity together with enhanced permeance. Scaling tests confirmed that the asymmetrically selective

membranes were able to retard gypsum scaling, paving a new paradigm for designing high performance NF membranes.

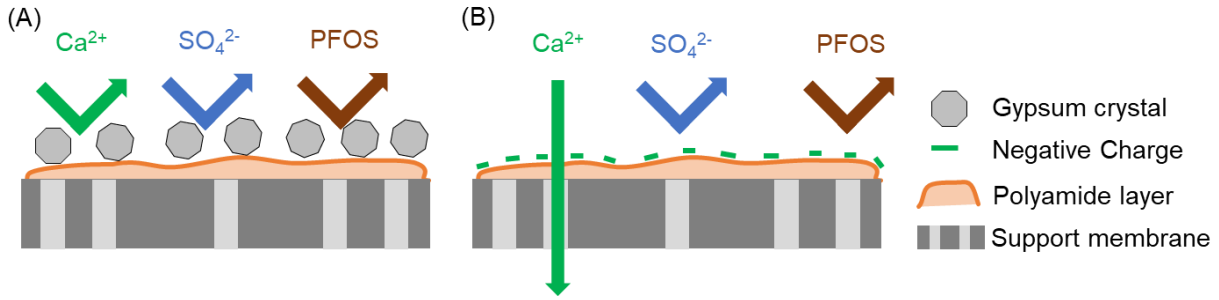

Figure 1. Schematic diagrams of (A) concurrent rejections of Ca^{2+}, SO_4^{2-} and PFOS with severe membrane scaling and (B) asymmetric rejections of Ca^{2+}, SO_4^{2-} and PFOS with reduced membrane scaling.

MATERIALS AND METHODS

Chemicals and materials. Piperazine (PIP, 99%), trimesoyl chloride (TMC, 98%), hexane (HPLC grade), and PFOS (>98%) were purchased from Sigma-Aldrich (St. Louis, MO, USA). Sodium sulfate, calcium chloride, sodium chloride, and sodium hydroxide were all analytical reagents (AR) and purchased from Dieckmann. GenX was received in the form of hexafluoropropylene oxide dimer acid (HFPO-DA, 330 Da) from Alfa Aesar. Perfluorooctanesulfonic acid (PFOS, 500 Da), perfluorooctanoic acid (PFOA, 414 Da), perfluorobutanesulfonic acid (PFBS, 300 Da) and perfluorobutanoic acid (PFBA, 214 Da) were purchased from Sigma-Aldrich. Poly(ethylene glycol) (PEG) with molecular weights of 200, 600, 1000, 2000, 4000 and 8000 Da were purchased from Aladdin Biochemical Technology Co., Ltd. (Shanghai, China).

Polyethersulfone (PES) ultrafiltration membrane with molecular weight cutoff of 150,000 Da (Microdyn Nadir, Germany) was used as the support membrane and washed in 25% (v/v) isopropanol/water solution for 1 h to remove any impurities. The PES membrane was then stored in deionized (DI) water. A commercial NF membrane, NF270 (FilmTec Corp., Minneapolis, MN), was received as flat sheet samples and washed by DI water prior to use.

Fabrication of thin-film composite nanofiltration membrane. The thin-film composite nanofiltration membrane was fabricated via typical interfacial polymerization between PIP and TMC as previously reported [37]. In brief, a PES support membrane (8 cm × 15 cm) was placed in a customized polycarbonate container with the skin layer upward. A 0.2 wt% PIP and 0.5 wt% NaOH mixture solution was gently poured onto the membrane and maintained for 3 min. The excess PIP/NaOH mixture solution was then removed by a rubber roller. After that, a hexane solution of 0.1 wt% TMC was poured onto the PES support membrane to react with PIP for 1

min. The resultant membrane (denoted as TFC-0.2 in accordance to the PIP concentration) was rinsed with hexane to wash out excess TMC, dried in an oven for 10 min at 60 °C and stored in DI water prior to testing. A control polyamide NF membrane was also fabricated following the same procedures without the addition of NaOH (denoted as TFC*). Other NF membranes with 0.1 and 0.02 wt% PIP concentrations (both with 0.5 wt% NaOH) were similarly prepared for comparison (denoted as TFC-0.1 and TFC-0.02).

Membrane characterization. Scanning electron microscopy (SEM, Hitachi S-4800, Germany) was conducted to examine the surface morphology of fabricated NF membranes at 5 keV. The membranes were first dried and sputter coated with gold to avoid charging effect prior to SEM analysis [38]. The polyamide layers of fabricated membranes were characterized by transmission electron microscopy (TEM, Philips CM100) as described in our previous study [39]. In detail, membrane samples were first embedded in a resin (Epon, Ted Pella, CA) and sectioned into ~100 nm thick TEM sections by an Ultracut E ultramicrotome (Reichert, Inc. Depew, NY). The sections were then placed on a copper grid and examined by TEM at 100 keV. Atomic force microscopy (AFM, Bruker, USA) was used to determine the surface roughness and polyamide thickness of fabricated membranes [32]. The value of root-mean-square roughness (Rq) and height profiling data were obtained using the Nanoscope Analysis software (Bruker, MA).

X-ray photoelectron spectroscopy (XPS) was conducted to analyze the elemental compositions on membrane surfaces using an SKL-12 spectrometer (Leybold, Sengyang, China) equipped with a VG CLAM 4 MCD electron energy analyzer [37]. Surface functional groups were measured by attenuated total reflection Fourier transform infrared (ATR FTIR) spectroscopy (Nicolet 6700, Thermo Fisher Scientific, Waltham, MA). Streaming zeta potential (ζ) measurements (SurPASS 3 Electrokinetic Analyzer, Anton PaarGmbH, Austria) were also

conducted to evaluate the surface charge over a pH range of 3–11 [37]. The water contact angles were measured using a goniometer equipped with a video capture device (Powereach, China). The membranes were dried in a vacuum oven for 24h prior to testing. A 5 μL of DI water droplet was placed on the membrane surfaces and stabilized for 10s. Each membrane sample was measured at five different locations and the average value was reported.

Membrane separation performance characterization. A cross-flow filtration setup was used to evaluate the membrane water flux and salt rejection as previously described [40]. The filtration cell had a membrane projection area of 2 cm × 4 cm, and the feed solution was circulated by a gear pump (Longer Pump, China) at a constant temperature of 25 ± 1 °C. The membranes were first compacted at 5 bar with DI water as feed solution for 1 h prior to each experiment. The pressure was reduced to 3.5 bar when measuring the water flux with feed solutions containing different solutes. The membrane flux was calculated based on Equation 1,

$$J = \frac{V}{A \times \Delta t} \quad (1)$$

where J (L m^{-2} h^{-1}) is the water flux, V (L) is the volume of permeate, A (m^2) is the membrane area, and Δt (h) is the testing time. The water permeance (A) was calculated based on Equation 2,

$$A = \frac{J}{\Delta P - \Delta \pi} \quad (2)$$

where A (L m^{-2} h^{-1} bar^{-1}) is the membrane water permeance, ΔP (bar) is the applied hydraulic pressure, and $\Delta \pi$ (bar) difference of osmotic pressure between feed and permeate.

Charged and neutral solutes were used to evaluate the separation performance of fabricated membranes. Single salt solutions of sodium chloride (NaCl), calcium chloride ($CaCl_2$), and sodium sulfate (Na_2SO_4) solutions, each at 1 g L^{-1}, was used for the charged solutes rejection tests. The rejection of salts was determined by measuring the conductivity of the feed and

permeate solutions (Ultrameter II, Myron Company, Carlsbad, CA) and calculated using Equation 3,

$$R = (1-\frac{C_p}{C_f}) \times 100\% \quad (3)$$

where R is the salt rejection, C_p is the permeate solution conductivity and C_f is the feed solution conductivity. An asymmetric rejection index was defined as the ratio of sulfate rejection over calcium rejection based on single salt rejection test to reflect the asymmetric separation capability of membranes. The sulfate rejection was obtained from the rejection of Na_2SO_4 solution (1 g L^{-1}), and calcium rejection was obtained from the rejection of $CaCl_2$ solution (1 g L^{-1}).

PEG (molecular weight of 200, 600, 1000, 2000, 4000 and 8000 Da) samples each at 0.2 g L^{-1} was used to evaluate the membrane separation performance following similar procedures to the salt rejection test. The permeate and feed concentrations of PEGs were determined by a total organic carbon (TOC) analyzer (TOC-L CPH, Shimadzu, Japan) [41].

The organic micropollutant rejections of PFOS, PFOA, GENx. PFBS and PFBA were also evaluated for fabricated membranes towards environmental remediation. After membrane compaction, retention of PFOS was examined with a feed solution containing 200 μg L^{-1} of PFOS in DI or 5 mM NaCl solution. The filtration process was continued for 3 h prior to the sample collection. The concentrations of the micropollutants in the feed and permeate samples were analyzed by UPLC-MS/MS (Agilent 1290 system. Santa Clara, CA) with C18 column (Eclipse Plus, Agilent), and the MS/ MS quantification was obtained by an API3200 mass detector (AB Sciex, MA) [42].

Scaling experiment. Scaling tests were performed without permeate recycling to mimic the volumetric concentrating of the brine and to evaluate the maximum allowable water recovery of

the fabricated membranes. For each test, a new membrane coupon was first compacted at 5 bar for 2 h with DI water (25 ± 1 °C) as the feed solution. After compaction, the feed solution was switched to a scaling solution composed of 10 mM (584 mg L^{-1}) NaCl, 20 mM (2220 mg L^{-1}) $CaCl_2$, and 10 mM (1420 mg L^{-1}) Na_2SO_4 at pH of 7.0 ± 0.1, corresponding to a saturation index of 0.7 with respect to gypsum. The contaminants were not added in the scaling solution due to high ionic strength for accurate measurement using UPLC-MS/MS. The hydraulic pressure was then adjusted to 4.4 bar to maintain an initial permeate water flux of ~ 80 L m^{-2} h^{-1}. The permeate was continuously weighed by an electronic balance and recorded by the computer at 1 min interval. The scaling test was continued until the permeate flux decreased below 20 L m^{-2} h^{-1} due to gypsum scaling. The water recovery was calculated by the mass ratio of the permeate over the initial feed. The commercial nanofiltration membrane NF270 was also tested as a benchmark following the above procedures, except at a pressure of 6.7 bar to obtain a similar initial permeate flux of 80 L m^{-2} h^{-1}. The Ca^{2+} and SO_4^{2-} concentrations in the feed and effluent solutions at different recoveries were quantified by an inductive coupled plasma optical emission spectrometer (ICP-OES, Optima 8 × 00, PerkinElmer) and ion chromatography (CDD-10Avp, Shimadzu).

RESULTS AND DISCUSSION

Mechanistic roles of NaOH on interfacial polymerization. The participation of NaOH during the interfacial polymerization significantly altered the polyamide morphology (Figure 2). The control TFC* membrane exhibited typical nodular surface morphology for PIP-based polyamide nanofiltration membranes (Figure 2A), which was similarly demonstrated in literature [43, 44]. With the addition of 0.5 wt% NaOH, the corresponding TFC-0.2 membrane exhibited a more pronounced nodular morphology of polyamide selective layer (Figure 2E). A previous

paper reported the formation of Turing-like structure under reduced interfacial polymerization rate [24]. In the current study, the accelerated interfacial polymerization process resulted in larger polyamide film thickness making typical nods morphology more pronounced. Future studies are needed to further investigate the underlining mechanisms regulating these morphological features. TEM images also showed thicker polyamide film for TFC-0.2 compared to TFC* (Figure 2B and 2F). The thickness of polyamide film for TFC-0.2 membrane was ~ 130 ± 1.5 nm compared to 15.0 ± 2.6 nm for TFC* membrane based on AFM analysis (Figure 2C and 2G), confirming the promoted interfacial polymerization with NaOH addition. The surface roughness of TFC-0.2 membrane is 9.9 ± 0.5 nm (Figure 2H), which is also slightly larger than 7.9 ± 0.8 nm for TFC* membrane (Figure 2D), indicating the promotional effect of NaOH as well. The polyamide formation is through condensation polymerization between amine and acyl chloride groups, which generates acid as a reaction byproduct [45]. The addition of NaOH neutralizes the acid generated from the IP reaction and therefore facilitates this condensation polymerization, leading to faster polyamide formation with potentially less defects. The change of polyamide thickness with NaOH addition was more significant than that for roughness, demonstrating that the promotion of interfacial polymerization was relatively uniform over the whole membrane surface.

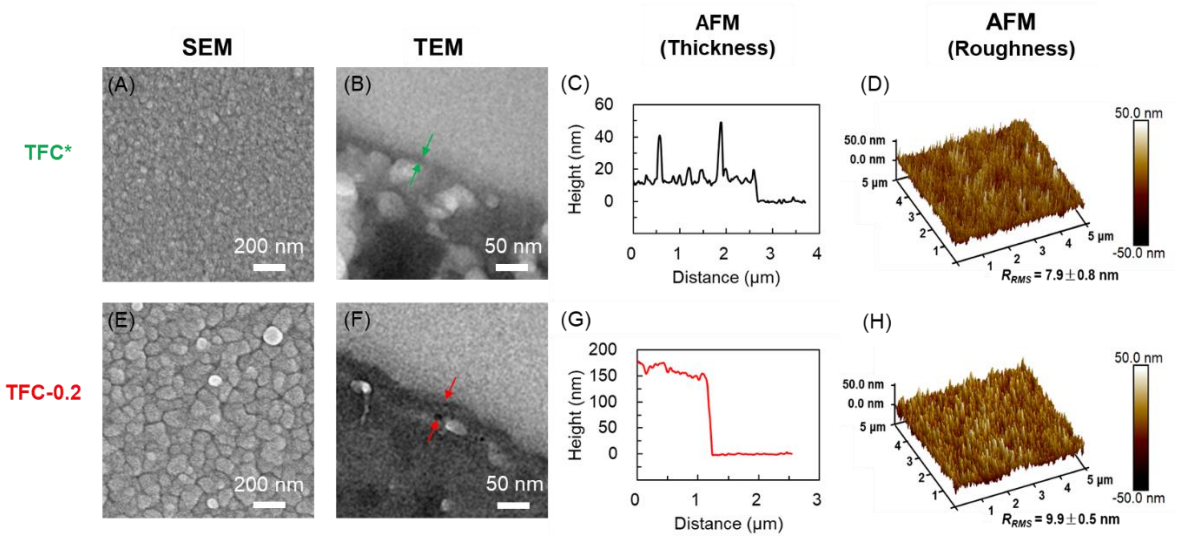

Figure 2. (A, E) SEM images of top membrane surface, (B, F) TEM cross sectional images of polyamide and polysulfone support, (C, G) AFM height profiling of polyamide and (D, H) AFM roughness of polyamide for TFC* and TFC-0.2 membranes. (The isolation of polyamide film was conducted by carefully removing the non-woven supported layer of NF membrane, followed by dimethylformamide washing repeatedly to dissolve the polyethersulfone. The isolated polyamide film was finally dried in an oven at 60 °C for 10 min for further AFM analysis [32].)

To further exemplify the promotional effect of NaOH, we also performed an interfacial reaction between PVA and TMC. Compared to the amine functional groups in PIP, PVA contains less reactive hydroxyl functional groups that normally do not form an intact rejection layer with TMC (Figure S3B) [46]. Nevertheless, a dense polymer film was formed in the current study when NaOH existed (Figure S3C), demonstrating the promotional effect in catalyzing the polymerization between hydroxyl and acyl chloride groups. A recent study also demonstrated that NaOH can catalyze the interfacial polymerization between glucose and TMC to fabricate nanofiltration membrane with ~95% Na_2SO_4 rejection [47].

In parallel to the catalysis effect, high NaOH concentration can also partially hydrolyze the polyamide rejection layer [45, 48]. This hydrolysis effect was confirmed by XPS results, which showed an increase of carboxyl groups from 26.3 ± 0.5% for control TFC* membrane to 34.1 ± 0.6% for TFC-0.2 membrane (Figure 3A and 3B). The major increase of carboxyl content can be

attributed to the hydrolysis of polyamide by NaOH. This hydrolysis further created a more negatively charged membrane surface due to the additional carboxyl functional groups, with the zeta potential curve for TFC-0.2 membrane becoming more negative compared to that for TFC* membrane (Figure 3C). Corresponding, the isoelectric point shifted from 3.8 for control TFC* membrane to 3.3 for the TFC-0.2 membrane. At the same time, zeta potential measurement could be affected by factors such as membrane morphology [49]. Therefore, we further measured the carboxyl group density for TFC* and TFC-0.2 membranes (Table S1). The COO^- density for TFC-0.2 was 99 ± 6 nm^{-2}, which was ~2.7 times of 33 ± 7 nm^{-2} for TFC* membrane, indicating the addition of sodium hydroxide during interfacial polymerization can greatly boost the membrane negative charge (Table S1). This hydrolysis effect would create a less dense rejection layer with enhanced negative charge, which promotes asymmetrical rejection of anions ($SO4^{2-}$ and PFOS) over cation (Ca^{2+}) with reduced scaling potential (Figure 1B).

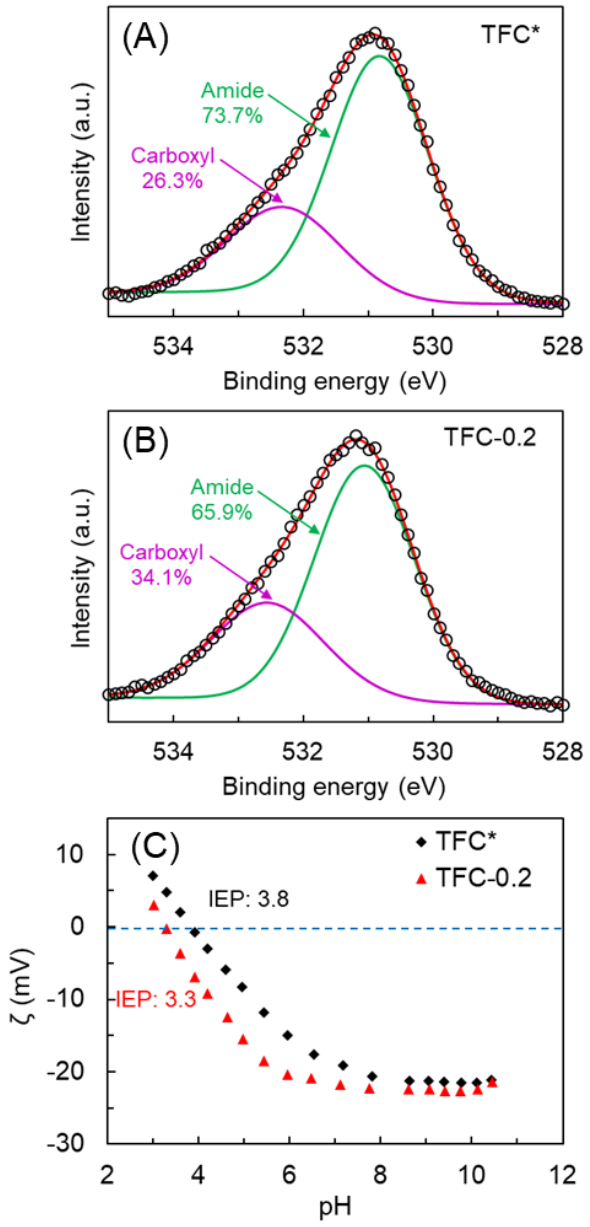

259

260 **Figure 3.** XPS spectra (A) O peak spectra with carboxyl and amide peaks fitting for TFC*
261 membrane and (B) O peak spectra with carboxyl and amide peaks fitting for TFC–0.2 membrane;
262 (C) Zeta potential curves for TFC* and TFC–0.2 membranes between pH 3 – 11 (The
263 background solution was 1 mM KCl).
264
265 PEG rejection tests were used to evaluate the effect of NaOH addition on the intrinsic
266 polyamide rejection property since their rejection is not influenced by membrane surface charge.
267 The rejections of PEGs were slightly lower for TFC-0.2 compared to control TFC* membrane,
268 indicating enlarged pore size for TFC-0.2 membrane (Figure 4). The pore size of TFC*

membrane is 0.55 ± 0.01 nm, and the pore size of TFC-0.2 membrane is 0.65 ± 0.03 nm (determined according to our previous method [40]). The pore size has slightly increased by addition of NaOH during interfacial polymerization. The possibility of potential defects formation was excluded through contaminants rejection test with increased rejections of all five emerging contaminants for TFC-0.2 membrane (Figure S7). Therefore, the higher rejection of TFC-0.2 membrane was likely due to reduced defects within polyamide layer, which is consistent with the promotional effect of NaOH on the growth of polyamide (Figure 2E) and PVA-TMC reaction (Figure S3C). Our study revealed the dual functions of NaOH on simultaneously (1) promoting polyamide formation with potentially reduced defects and (2) hydrolyzing polyamide layer with enhanced negative surface charge. This strategy ensures high removal of target contaminants (PFOS and SO_4^{2-} anions). At the same time, it diverts Ca^{2+} cations through the looser and more negatively charged membrane.

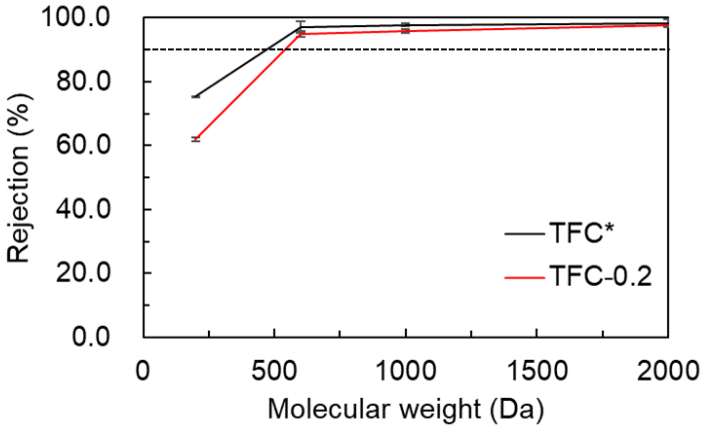

Figure 4. PEG rejections with different molecular weight (200, 600, 1000 and 2000 Da) for TFC* and TFC–0.2 membranes. (The rejection test was separately conducted for each PEG at an operating pressure of 3.5 bar and a feed concentration of 0.2 g L^{-1}).

Membrane permeance and separation property. The pure water permeance for TFC-0.2 membrane was lower compared to control TFC* membrane (Figure 5A) due to the promoted

polyamide growth with increased water permeation resistance (Figure 2E). The promotional effect of NaOH could allow the use of lower PIP concentrations to achieve optimized membrane water permeance without significant loss of rejection. The pure water permeance increased to 29.0 ± 0.7 L $m^{-2} h^{-1} bar^{-1}$ (TFC-0.1) and 54.0 ± 0.5 L $m^{-2} h^{-1} bar^{-1}$ (TFC-0.02) compared to 11.5 ± 0.2 L $m^{-2} h^{-1} bar^{-1}$ (TFC-0.2) (Figure 5A). In addition, the pure water permeance of TFC-0.1 and TFC-0.02 were respectively 2.1 and 3.9 times of that for commercial NF270 (Figure 5A), demonstrating great potential for practical applications.

Asymmetric rejection between calcium and sulfate was also accomplished with NaOH assisted interfacial polymerization. For Na_2SO_4, both TFC* and TFC-0.2 membranes exhibited high rejections (> 98%) due to the relatively large size and negative charge of sulfate ions (Figure 5B) [50]. On the contrary, the $CaCl_2$ rejection for TFC-0.2 decreased to 25 ± 0.7% versus 44 ± 7% for TFC* membrane (Figure 5B). This lower rejection of $CaCl_2$ for TFC-0.2 mainly resulted from its negative surface charge and a more porous polyamide backbone due to the hydrolysis effect of NaOH. Therefore, the selectively passing of Ca^{2+} enabled decreased $CaCl_2$ rejection, proving the successful tuning of the asymmetric selectivity.

Reducing PIP concentration to 0.1 wt% (TFC-0.1) obtained even lower $CaCl_2$ rejection (11.4 ± 0.6%) by generating a looser polyamide network, which was much lower than 41.1 ± 0.3% for NF270 (Figure 5B). Its Na_2SO_4 rejection remained relatively high (96.1 ± 0.6%), which can be attributed to the favorable electrostatic repulsion. Further lowering PIP concentration to 0.02% (TFC-0.02) achieved even lower $CaCl_2$ rejection (3 ± 0.1%) accompanied by decreased Na_2SO_4 rejection (53.3 ± 0.1%). Conventional membrane modification methods to enlarge membrane pore size by decreasing PIP concentration often tend to generate defect sites, leading to significantly reduced solutes rejection [51, 52]. Due to this low Na_2SO_4 rejection, this membrane

311 is not suitable for the targeted asymmetrical removal of contaminants in the current study. In all
312 cases, the PFOS rejection was maintained over 90%. The TFC-0.2 and TFC-0.1 membranes also
313 showed increased rejections for other emerging contaminants compared to that for TFC*
314 membrane (Figure S7), which might result from the minimized defects and enhanced hydrolysis
315 in polyamide rejection layer during sodium hydroxide promoted interfacial polymerization. The
316 asymmetric rejection index, defined as rejection ratio of Na_2SO_4 over $CaCl_2$, was 8.5 ± 0.6 for
317 TFC-0.1 meaning 8 times more SO_4^{2-} was rejected over Ca^{2+} (Figure 5C). In contrast, both the
318 conventional TFC* and the commercial NF270 had an asymmetric rejection index of 2-2.5,
319 indicating less efficiency in separating SO_4^{2-} from Ca^{2+}. Both TFC-0.1 and TFC-0.02
320 membranes surpassed the upper bound compared to existing literature on nanofiltration
321 membranes in terms of water permeance and asymmetric separation performance (Figure 5D).
322 The asymmetric rejection index was selected as it is straightforward to show the separation
323 effectiveness between sulfate and calcium. At the same time, we also present the B_{Ca}^{2+}/B_{SO4}^{2-}
324 values of all membranes in Figure S8 in the supporting information. Although the ratio of solute
325 permeance coefficients is often used to characterize solute/solute selectivity, it is worthwhile to
326 note that a high B_{Ca}^{2+}/B_{SO4}^{2-} does not guarantee a good separation of the two species. For
327 example, when both B_{Ca}^{2+} and B_{SO4}^{2-} are sufficiently small (<< water flux J), the two species are
328 both well rejected by the membrane since the intrinsic rejection of a membrane is given by
329 J/(J+B).[53] High anion/cation asymmetrical rejection was preferred in current study. However,
330 in some other applications (e.g., water softening), a high cation/anion asymmetrical rejection
331 might be needed (i.e., anion/cation asymmetrical rejection << 1).

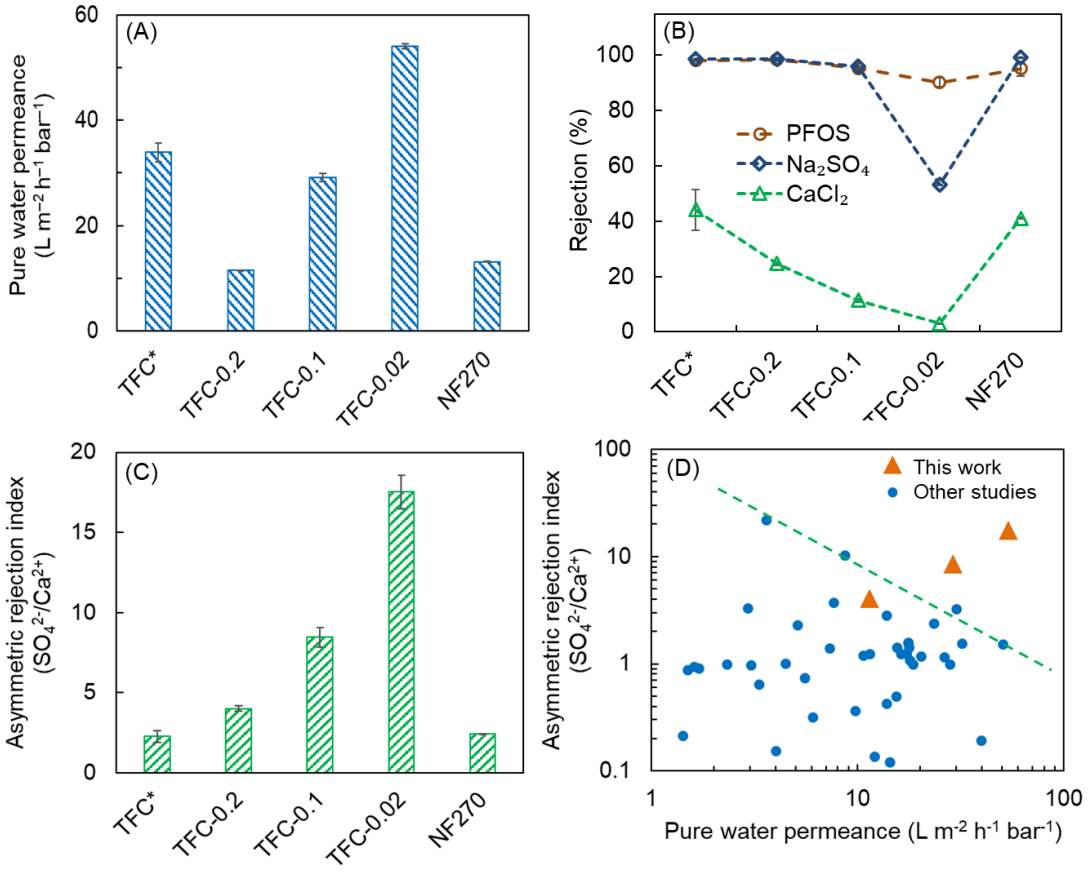

Figure 5. (A) Pure water permeance, (B) Na_2SO_4, $CaCl_2$ and PFOS rejections, (C) Asymmetric rejection index (SO_4^{2-}/Ca^{2+}) for TFC*, TFC–0.2, TFC–0.1, TFC–0.02 and NF270 membranes and (D) Comparison of asymmetric rejection performance of fabricated membranes with the upper bound trade-off for TFC membranes in literature. (The filtration experiments were conducted at an operating pressure of 3.5 bar; The Na_2SO_4 and $CaCl_2$ aqueous solutions were separately tested each at 1 g L^{-1}; The PFOS rejections were separately tested at a concentration of 200 μg L^{-1}).

Water recovery with asymmetrically selective membrane upon scaling. The TFC-0.1 membrane was adopted for the scaling test and benchmarked with the commercial NF270 membrane based on the comparable PFOS rejections. Without permeate recycling, the water fluxes of TFC-0.1 and NF270 membranes gradually attenuated (Figure 6A) due to the increasing osmotic pressure from the concentrated feed solutions over time. For each membrane, the water flux declined sharply when the water recovery exceeded certain threshold value, which was

caused by severe membrane scaling (Figure S12A and S12B). Nevertheless, the threshold water recovery for TFC-0.1 membrane was ~60%, which was much higher than that for commercial NF270 of ~40% (Figure 6A). The delayed scaling property of TFC-0.1 membrane was more evidently demonstrated by the scattered small size gypsum crystals on membrane surface at 40% water recovery (Figure 6B), while NF270 membrane surface was mostly covered by large pieces of gypsum crystal clusters (Figure 6C).

The difference in water recovery mainly resulted from the selective passage of Ca^{2+} for TFC-0.1 membrane, which was the main component for gypsum scaling [54]. The permeate Ca^{2+} concentration for TFC-0.1 was about two times higher than that for NF270 at different water recoveries (Figure 6D). The selective passage of Ca^{2+} enabled a greater amount of permeate water to be produced before reaching critical supersaturation with respect to gypsum. The permeate concentrations of SO_4^{2-} remained very low before the occurrence of severe scaling (Figure 6E). However, the occurrence of membrane scaling caused dramatically increased SO_4^{2-} passage through both membranes, which can be attributed to the cake-enhanced concentration polarization inside the gypsum cake layer [55]. Overall, the TFC-0.1 membrane with improved asymmetric selectivity of Ca^{2+} over SO_4^{2-} (Figure 3C) effectively enhanced the maximum water recovery under scaling condition (Figure 4A). Besides higher water recovery, the highly permeable TFC-0.1 membrane can be operated at lower pressure of 4.4 bar compared to 6.7 bar for NF270 with a comparable water flux, which could also help lower the energy consumption.

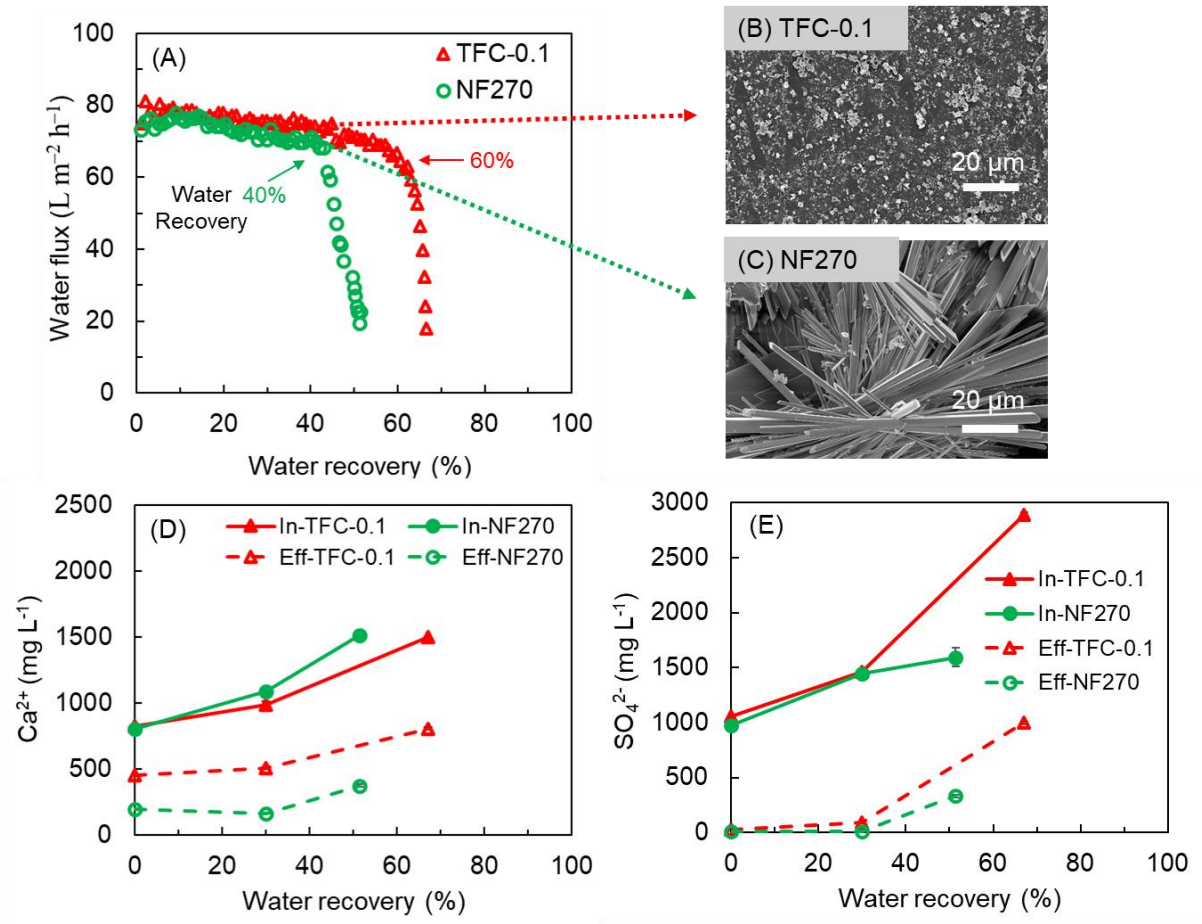

366

367 **Figure 6.** (A) Water flux decline curves for TFC–0.1 and NF270 membranes during scaling tests
368 at different recoveries, (B) Ca^{2+} and (C) SO_4^{2-} concentrations in the influent (In) and effluent (Eff)
369 solutions for TFC–0.1 and NF270 membranes. (Operating pressure of 4.4 bar for TFC-0.1 and
370 6.7 bar for NF270; scaling solution composed of 10 mM (584 mg L^{-1}) NaCl, 20 mM (2220 mg
371 L^{-1}) $CaCl_2$, and 10 mM (1420 mg L^{-1}) Na_2SO_4 (saturation index of 0.7) at pH of 7.0 ± 0.1)
372

373 **Implications.** In this study, a simple promoted interfacial polymerization with NaOH was
374 introduced to tailor the membrane asymmetric selectivity of calcium over sulfate ions to reduce
375 scaling potential towards high water recovery. The dual functions of NaOH in promoting
376 polyamide polymerization with less defects and enhanced hydrolysis were fine tuned to enable
377 comparable PFOS removal compared to commercial NF270 membrane, while yielding higher
378 water permeance and lower gypsum scaling potential. The designed polyamide membranes
379 demonstrated strong potential for high water recovery in groundwater remediation contaminated

with emerging pollutants. While the definition of the optimal ratio of anion/cation asymmetrical rejection is beyond the current scope of this study, further investigations are still needed to study the ratio of membrane anion/cation asymmetrical rejection in practical groundwater remediation. The exemplified strategy of NaOH promoted interfacial polymerization also shed light in tailoring membrane asymmetric selectivity at low cost and can be readily applied for industrial manufacture.

SUPPORTING INFORMATION

This material is available free of charge via the Internet at http://pubs.acs.org.

Additional filtration tests, XPS spectra and zeta analysis; Carboxylic group characterization, SEM images of PVA membranes; SEM images of membranes with varied NaOH concentration; Contact angles; FTIR spectra; SEM and EDS mapping of surface scaling. A table of references for upper-bound plot.

AUTHOR INFORMATION

Corresponding Authors

Zhe Yang - Department of Civil Engineering, The University of Hong Kong, Hong Kong 999077, P. R. China; ORCID 0000-0003-0753-3902; Tel: +852-2857 8470; E-mail address: zheyang@connect.hku.hk

Chuyang Y. Tang - Department of Civil Engineering, The University of Hong Kong, Hong Kong 999077, P. R. China; ORCID 0000-0002-7932-6462; Tel: +852-2859 1976; E-mail address: tangc@hku.hk

Authors

Wulin Yang - College of Environmental Sciences and Engineering, Peking University, Beijing 100871, China; Department of Civil Engineering, The University of Hong Kong, Hong Kong 999077, P. R. China; ORCID 0000-0003-3590-5080

Li Long - Department of Civil Engineering, The University of Hong Kong, Hong Kong 999077, P. R. China; ORCID 0000-0002-7951-3276

Hao Guo - Department of Civil Engineering, The University of Hong Kong, Hong Kong 999077, P. R. China; ORCID 0000-0002-0688-5431

Chenyue Wu - Department of Civil Engineering, The University of Hong Kong, Hong Kong 999077, P. R. China; ORCID 0000-0002-1846-8192

Shenghua Zhou - Department of Civil Engineering, The University of Hong Kong, Hong Kong 999077, P. R. China

Ying Mei - Department of Civil Engineering, The University of Hong Kong, Hong Kong 999077, P. R. China; ORCID 0000-0002-1168-3834

Lu Elfa Peng - Department of Civil Engineering, The University of Hong Kong, Hong Kong 999077, P. R. China; ORCID 0000-0002-3223-4608

Wanbin Li - Department of Civil Engineering, The University of Hong Kong, Hong Kong 999077, P. R. China; Guangdong Key Laboratory of Environmental Pollution and Health, School of Environment, Jinan University, Guangzhou 511443, China; ORCID 0000-0003-2460-168X

DECLARATION OF COMPETING INTEREST (COI)

The authors declare that they have no known competing financial interests or personal relationships that could have appeared to influence the work reported in this paper.

CRediT authorship contribution statement

Wulin Yang: Investigation, Methodology, Data curation, Formal analysis, Writing - original draft.

Li Long: Investigation, Methodology, Data curation, Formal analysis.

Hao Guo: Methodology, Formal analysis.

Chenyue Wu: Methodology, Formal analysis.

Shenghua Zhou: Methodology, Formal analysis.

Ying Mei: Methodology, Formal analysis.

Lu Elfa Peng: Methodology, Formal analysis.

Wenyu Liu: Methodology, Formal analysis.

Zhe Yang: Supervision, Conceptualization, Writing - review & editing.

Wanbin Li: Methodology, Formal analysis.

Chuyang Tang: Supervision, Conceptualization, Writing - review & editing.

ACKNOWLEDGEMENTS

This work was supported by (1) the National Key Research and Development Program of China (Grant No. 2021YFA1202500), (2) the RGC Postdoctoral Fellowship from the Research Grants Council of the Hong Kong Special Administrative Region, China (PDFS2021-7S01), and (3) the Senior Research Fellow Scheme of Research Grants Council of the Hong Kong Special Administrative Region, China (Project # SRFS2021-7S04).

REFERENCES

[1] X. Xiao, B.A. Ulrich, B. Chen, C.P. Higgins, Sorption of Poly- and Perfluoroalkyl Substances (PFASs) Relevant to Aqueous Film-Forming Foam (AFFF)-Impacted Groundwater by Biochars and Activated Carbon, Environ. Sci. Technol. 51(11) (2017) 6342-6351.

[2] M. Stuart, D. Lapworth, E. Crane, A. Hart, Review of risk from potential emerging contaminants in UK groundwater, Sci. Total Environ. 416 (2012) 1-21.

[3] E.F. Houtz, C.P. Higgins, J.A. Field, D.L. Sedlak, Persistence of Perfluoroalkyl Acid Precursors in AFFF-Impacted Groundwater and Soil, Environ. Sci. Technol. 47(15) (2013) 8187-8195.

[4] L. Gobelius, J. Hedlund, W. Dürig, R. Tröger, K. Lilja, K. Wiberg, L. Ahrens, Per- and Polyfluoroalkyl Substances in Swedish Groundwater and Surface Water: Implications for Environmental Quality Standards and Drinking Water Guidelines, Environ. Sci. Technol. 52(7) (2018) 4340-4349.

[5] K.A. Barzen-Hanson, S.C. Roberts, S. Choyke, K. Oetjen, A. McAlees, N. Riddell, R. McCrindle, P.L. Ferguson, C.P. Higgins, J.A. Field, Discovery of 40 Classes of Per- and Polyfluoroalkyl Substances in Historical Aqueous Film-Forming Foams (AFFFs) and AFFF-Impacted Groundwater, Environ. Sci. Technol. 51(4) (2017) 2047-2057.

[6] J.J. MacInnis, I. Lehnherr, D.C.G. Muir, K.A. St. Pierre, V.L. St. Louis, C. Spencer, A.O. De Silva, Fate and Transport of Perfluoroalkyl Substances from Snowpacks into a Lake in the High Arctic of Canada, Environ. Sci. Technol. 53(18) (2019) 10753-10762.

[7] W. Qiao, R. Li, T. Tang, A.A. Zuh, Removal, distribution and plant uptake of perfluorooctane sulfonate (PFOS) in a simulated constructed wetland system, Front. Environ. Sci. Eng. 15(2) (2020) 20.

[8] F. Xiao, M.F. Simcik, T.R. Halbach, J.S. Gulliver, Perfluorooctane sulfonate (PFOS) and perfluorooctanoate (PFOA) in soils and groundwater of a US metropolitan area: migration and implications for human exposure, Water Res. 72 (2015) 64-74.

[9] C. Kunacheva, S. Fujii, S. Tanaka, S.T.M.L.D. Seneviratne, N.P.H. Lien, M. Nozoe, K. Kimura, B.R. Shivakoti, H. Harada, Worldwide surveys of perfluorooctane sulfonate (PFOS) and perfluorooctanoic acid (PFOA) in water environment in recent years, Water Sci. Technol. 66(12) (2012) 2764-2771.

[10] N. Briels, T.M. Ciesielski, D. Herzke, V.L.B. Jaspers, Developmental Toxicity of Perfluorooctanesulfonate (PFOS) and Its Chlorinated Polyfluoroalkyl Ether Sulfonate Alternative F-53B in the Domestic Chicken, Environ. Sci. Technol. 52(21) (2018) 12859-12867.

[11] F. Wang, W. Liu, Y. Jin, J. Dai, W. Yu, X. Liu, L. Liu, Transcriptional Effects of Prenatal and Neonatal Exposure to PFOS in Developing Rat Brain, Environ. Sci. Technol. 44(5) (2010) 1847-1853.

[12] Á. Soriano, D. Gorri, A. Urtiaga, Efficient treatment of perfluorohexanoic acid by nanofiltration followed by electrochemical degradation of the NF concentrate, Water Res. 112 (2017) 147-156.

[13] J. Wang, L. Wang, C. Xu, R. Zhi, R. Miao, T. Liang, X. Yue, Y. Lv, T. Liu, Perfluorooctane sulfonate and perfluorobutane sulfonate removal from water by nanofiltration membrane: The roles of solute concentration, ionic strength, and macromolecular organic foulants, Chem. Eng. J. 332 (2018) 787-797.

[14] C. Boo, Y. Wang, I. Zucker, Y. Choo, C.O. Osuji, M. Elimelech, High Performance Nanofiltration Membrane for Effective Removal of Perfluoroalkyl Substances at High Water Recovery, Environ. Sci. Technol. 52(13) (2018) 7279-7288.
[15] C.Y. Tang, Q.S. Fu, C.S. Criddle, J.O. Leckie, Effect of flux (transmembrane pressure) and membrane properties on fouling and rejection of reverse osmosis and nanofiltration membranes treating perfluorooctane sulfonate containing wastewater, Environ. Sci. Technol. 41(6) (2007) 2008-2014.
[16] R. Dai, H. Han, Y. Zhu, X. Wang, Z. Wang, Tuning the primary selective nanochannels of MOF thin-film nanocomposite nanofiltration membranes for efficient removal of hydrophobic endocrine disrupting compounds, Front. Environ. Sci. Eng. 16(4) (2021) 40.
[17] C. Zhao, T. Zhang, G. Hu, J. Ma, R. Song, J. Li, Efficient removal of perfluorooctane sulphonate by nanofiltration: Insights into the effect and mechanism of coexisting inorganic ions and humic acid, J. Membr. Sci. 610 (2020) 118176.
[18] T. Wang, C. Zhao, P. Li, Y. Li, J. Wang, Fabrication of novel poly(m-phenylene isophthalamide) hollow fiber nanofiltration membrane for effective removal of trace amount perfluorooctane sulfonate from water, J. Membr. Sci. 477 (2015) 74-85.
[19] C.Y. Tang, Q.S. Fu, A.P. Robertson, C.S. Criddle, J.O. Leckie, Use of Reverse Osmosis Membranes to Remove Perfluorooctane Sulfonate (PFOS) from Semiconductor Wastewater†, Environ. Sci. Technol. 40(23) (2006) 7343-7349.
[20] F. Beyer, B.M. Rietman, A. Zwijnenburg, P. van den Brink, J.S. Vrouwenvelder, M. Jarzembowska, J. Laurinonyte, A.J.M. Stams, C.M. Plugge, Long-term performance and fouling analysis of full-scale direct nanofiltration (NF) installations treating anoxic groundwater, J. Membr. Sci. 468 (2014) 339-348.
[21] K.D. Cobry, Z. Yuan, J. Gilron, V.M. Bright, W.B. Krantz, A.R. Greenberg, Comprehensive experimental studies of early-stage membrane scaling during nanofiltration, Desalination 283 (2011) 40-51.
[22] H.M. Krieg, S.J. Modise, K. Keizer, H.W.J.P. Neomagus, Salt rejection in nanofiltration for single and binary salt mixtures in view of sulphate removal, Desalination 171(2) (2005) 205-215.
[23] K.L. Tu, L.D. Nghiem, A.R. Chivas, Coupling effects of feed solution pH and ionic strength on the rejection of boron by NF/RO membranes, Chem. Eng. J. 168(2) (2011) 700-706.
[24] Z. Tan, S. Chen, X. Peng, L. Zhang, C. Gao, Polyamide membranes with nanoscale Turing structures for water purification, Science 360(6388) (2018) 518-521.
[25] C.M. Galanakis, G. Fountoulis, V. Gekas, Nanofiltration of brackish groundwater by using a polypiperazine membrane, Desalination 286 (2012) 277-284.
[26] Y. Song, T. Li, J. Zhou, Z. Li, C. Gao, Analysis of nanofiltration membrane performance during softening process of simulated brackish groundwater, Desalination 399 (2016) 159-164.
[27] J. Wang, L. Wang, R. Miao, Y. Lv, X. Wang, X. Meng, R. Yang, X. Zhang, Enhanced gypsum scaling by organic fouling layer on nanofiltration membrane: Characteristics and mechanisms, Water Res. 91 (2016) 203-213.
[28] C.A.C. van de Lisdonk, J.A.M. van Paassen, J.C. Schippers, Monitoring scaling in nanofiltration and reverse osmosis membrane systems, Desalination 132(1) (2000) 101-108.
[29] D.L. Sedlak, The Unintended Consequences of the Reverse Osmosis Revolution, Environ. Sci. Technol. 53(8) (2019) 3999-4000.
[30] Y. Yu, C. Zhao, L. Yu, P. Li, T. Wang, Y. Xu, Removal of perfluorooctane sulfonates from water by a hybrid coagulation–nanofiltration process, Chem. Eng. J. 289 (2016) 7-16.

[31] J. Luo, Y. Wan, Effects of pH and salt on nanofiltration—a critical review, J. Membr. Sci. 438 (2013) 18-28.
[32] L. Long, C. Wu, Z. Yang, C.Y. Tang, Carbon Nanotube Interlayer Enhances Water Permeance and Antifouling Performance of Nanofiltration Membranes: Mechanisms and Experimental Evidence, Environ. Sci. Technol. 56(4) (2022) 2656-2664.
[33] W. Zhang, N. Li, X. Zhang, Surface-engineered sulfonation of ion-selective nanofiltration membrane with robust scaling resistance for seawater desalination, J. Membr. Sci. 644 (2022) 120191.
[34] W. Zhang, X. Zhang, Effective inhibition of gypsum using an ion–ion selective nanofiltration membrane pretreatment process for seawater desalination, J. Membr. Sci. 632 (2021) 119358.
[35] Z. Yang, H. Guo, C.Y. Tang, The upper bound of thin-film composite (TFC) polyamide membranes for desalination, J. Membr. Sci. 590 (2019) 117297.
[36] X. Song, B. Gan, S. Qi, H. Guo, C.Y. Tang, Y. Zhou, C. Gao, Intrinsic Nanoscale Structure of Thin Film Composite Polyamide Membranes: Connectivity, Defects, and Structure-Property Correlation, Environ. Sci. Technol. 54(6) (2020) 3559-3569.
[37] Z. Yang, Y. Wu, H. Guo, X.-H. Ma, C.-E. Lin, Y. Zhou, B. Cao, B.-K. Zhu, K. Shih, C.Y. Tang, A novel thin-film nano-templated composite membrane with in situ silver nanoparticles loading: Separation performance enhancement and implications, J. Membr. Sci. 544 (2017) 351-358.
[38] Z. Yang, H. Guo, Z.-k. Yao, Y. Mei, C.Y. Tang, Hydrophilic Silver Nanoparticles Induce Selective Nanochannels in Thin Film Nanocomposite Polyamide Membranes, Environ. Sci. Technol. 53(9) (2019) 5301-5308.
[39] Z. Yang, Y. Wu, J. Wang, B. Cao, C.Y. Tang, In Situ Reduction of Silver by Polydopamine: A Novel Antimicrobial Modification of a Thin-Film Composite Polyamide Membrane, Environ. Sci. Technol. 50(17) (2016) 9543-9550.
[40] Z. Yang, Z.-w. Zhou, H. Guo, Z. Yao, X.-h. Ma, X. Song, S.-P. Feng, C.Y. Tang, Tannic Acid/Fe3+ Nanoscaffold for Interfacial Polymerization: Toward Enhanced Nanofiltration Performance, Environ. Sci. Technol. 52(16) (2018) 9341-9349.
[41] M. Dubois, K.A. Gilles, J.K. Hamilton, P.A. Rebers, F. Smith, Colorimetric Method for Determination of Sugars and Related Substances, Anal. Chem. 28(3) (1956) 350-356.
[42] H. Guo, J. Zhang, L.E. Peng, X. Li, Y. Chen, Z. Yao, Y. Fan, K. Shih, C.Y. Tang, High-Efficiency Capture and Recovery of Anionic Perfluoroalkyl Substances from Water Using PVA/PDDA Nanofibrous Membranes with Near-Zero Energy Consumption, Environ. Sci. Technol. Lett. 8(4) (2021) 350-355.
[43] C.Y. Tang, Y.-N. Kwon, J.O. Leckie, Effect of membrane chemistry and coating layer on physiochemical properties of thin film composite polyamide RO and NF membranes: II. Membrane physiochemical properties and their dependence on polyamide and coating layers, Desalination 242(1-3) (2009) 168-182.
[44] Y. Hao, Q. Li, B. He, B. Liao, X. Li, M. Hu, Y. Ji, Z. Cui, M. Younas, J. Li, An ultrahighly permeable-selective nanofiltration membrane mediated by an in situ formed interlayer, J. Mater. Chem. A 8(10) (2020) 5275-5283.
[45] L.E. Peng, Z. Yao, X. Liu, B. Deng, H. Guo, C.Y. Tang, Tailoring Polyamide Rejection Layer with Aqueous Carbonate Chemistry for Enhanced Membrane Separation: Mechanistic Insights, Chemistry-Structure-Property Relationship, and Environmental Implications, Environ. Sci. Technol. 53(16) (2019) 9764-9770.

[46] X.-H. Ma, Z. Yao, Z. Yang, H. Guo, Z. Xu, C.Y. Tang, M. Elimelech, Nanofoaming of Polyamide Desalination Membranes to Tune Permeability and Selectivity, Environ. Sci. Technol. Lett. 5(2) (2018) 123-130.
[47] J. Zheng, Y. Liu, J. Zhu, P. Jin, T. Croes, A. Volodine, S. Yuan, B. Van der Bruggen, Sugar-based membranes for nanofiltration, J. Membr. Sci. 619 (2021) 118786.
[48] K. Hashiba, S. Nakai, M. Ohno, W. Nishijima, T. Gotoh, T. Iizawa, Deterioration Mechanism of a Tertiary Polyamide Reverse Osmosis Membrane by Hypochlorite, Environ. Sci. Technol. 53(15) (2019) 9109-9117.
[49] B.J. Pedimonte, T. Moest, T. Luxbacher, C. von Wilmowsky, T. Fey, K.A. Schlegel, P. Greil, Morphological zeta-potential variation of nanoporous anodic alumina layers and cell adherence, Acta Biomater. 10(2) (2014) 968-974.
[50] L. Meihong, Y. Sanchuan, Z. Yong, G. Congjie, Study on the thin-film composite nanofiltration membrane for the removal of sulfate from concentrated salt aqueous: Preparation and performance, J. Membr. Sci. 310(1) (2008) 289-295.
[51] S. Yuan, G. Zhang, J. Zhu, N. Mamrol, S. Liu, Z. Mai, P. Van Puyvelde, B. Van der Bruggen, Hydrogel Assisted Interfacial Polymerization for Advanced Nanofiltration Membranes, J. Mater. Chem. A. 8 (2020) 3238-3245.
[52] W. Wang, G. Li, One-step fabrication of high selective hollow fiber nanofiltration membrane module, Fibers Polym. 11(7) (2010) 1041-1048.
[53] Z. Yang, L. Long, C. Wu, C.Y. Tang, High Permeance or High Selectivity? Optimization of System-Scale Nanofiltration Performance Constrained by the Upper Bound, ACS EST Engg. 2(3) (2022) 377-390.
[54] B. Mi, M. Elimelech, Gypsum Scaling and Cleaning in Forward Osmosis: Measurements and Mechanisms, Environ. Sci. Technol. 44(6) (2010) 2022-2028.
[55] E.M.V. Hoek, M. Elimelech, Cake-Enhanced Concentration Polarization: A New Fouling Mechanism for Salt-Rejecting Membranes, Environ. Sci. Technol. 37(24) (2003) 5581-5588.